JCIS Open 11 (2023) 100089

Contents lists available at ScienceDirect

JCIS Open

journal homepage: www.journals.elsevier.com/jcis-open

Unusual gold nanoparticle-antibody interactions

Helena Mateos [a,*], Antonia Mallardi [b], Esther Serrano-Pertierra [c], María Carmen Blanco-López [c], Margherita Izzi [a], Nicola Cioffi [a], Gerardo Palazzo [a]

[a] Dipartimento di Chimica, Università di Bari and CSGI (Consorzio Interuniversitario per lo Sviluppo dei Sistemi a Grande Interfase), 70125, Bari, Italy
[b] CNR-IPCF, Istituto per i Processi Chimico-Fisici, 70125, Bari, Italy
[c] Departamento de Química Física y Analítica & Instituto Universitario de Biotecnología de Asturias, Universidad de Oviedo, 33006, Oviedo, Spain

ARTICLE INFO

Keywords:
Colloidal stability
Protein corona
DLS
TEM
Antibody aggregation

ABSTRACT

The formation of an antibody (Ab) protein corona surrounding gold nanoparticles (AuNPs) is a crucial step in the design of immunological assays. The Ab corona stabilizes AuNPs, preventing their aggregation even at high ionic strength, and can be achieved by simply mixing Abs and AuNPs. In this paper, we report the unusual interactions between AuNPs and the antibody against L1 Cell Adhesion Molecule (L1CAM) purified from rabbits.

We have observed that at low ionic strength, the addition of a wide range of concentrations of rabbit monoclonal Abs against L1CAM protein immediately causes the coagulation of citrate-capped gold nanoparticles. This finding is surprising since the addition of proteins to colloidal gold usually forms a stable protein corona. The combination of extinction spectra, dynamic light scattering (DLS), and transmission electron microscopy (TEM) measurements reveals the presence of small clusters of AuNPs coated by the antibodies, as well as micron-sized antibody aggregates. Furthermore, static light scattering measurements demonstrate that Ab self-interactions are attractive (with a negative second virial coefficient, B2) and induce very slow Ab self-aggregation over several months. Overall, these results indicate that, at low ionic strength, the presence of AuNPs enhances Ab-Ab interactions, leading to their rapid aggregation. Simultaneously, the self-aggregation of the antibodies coating the AuNPs results in the formation of nanoparticle clusters.

The addition of NaCl to increase the ionic strength fully reverses the coagulation of AuNPs (the Ab-coated AuNPs repel each other) and dissolves the Ab aggregates (the Ab interactions become repulsive, with a positive B2). The AuNPs-induced enhancement of the aggregation process can be explained by considering that the highly favorable binding of Abs on the gold surface compensates for the entropic penalty associated with Ab-Ab aggregation.

The phenomenon we observed is specific to anti-L1CAM purified from rabbits and aligns with very old reports on AuNP coagulation induced specifically by the immunoglobulins present in the cerebrospinal fluid of patients suffering from neurosyphilis or multiple sclerosis (C. Lange Zeitschr. Chemotherap., 1912, 1, 44). It is reasonable to hypothesize that other antibodies exhibit this unusual behavior, so this work may aid in the interpretation of "anomalous" results that might otherwise be attributed to errors in fine-tuning AuNPs-Abs conjugation protocols.

1. Introduction

Gold labeling of antibodies (Ab) is a standard technique in the development of diagnostic tools, which utilizes the red color of gold nanoparticles (AuNPs) to indicate their binding to the target analyte. The size and colour of AuNPs can be controlled and adjusted by varying the synthesis conditions. Due to their excellent colloidal stability, they are widely employed as colorimetric reporters in immunological assays, offering strong stability and good optical signals.

The proper conjugation of antibodies to nanoparticles is fundamental to many of these techniques. NPs and proteins can bind to each other in two different ways: through direct covalent attachment between proteins and the surface of NPs, or through non-covalent interactions. Covalent interactions form highly stable complexes and can alter the protein conformation. Non-covalent interactions include van der Waals forces, hydrogen bonding, electrostatic and hydrophobic interactions, with electrostatic interaction being the most common [1]. In the case of antibodies, their spontaneous adsorption onto AuNPs is initially driven by

* Corresponding author.
E-mail address: Helena.mateos@uniba.it (H. Mateos).

https://doi.org/10.1016/j.jciso.2023.100089
Received 24 February 2023; Received in revised form 24 May 2023; Accepted 12 June 2023

electrostatic interaction [2] and subsequently, due to the large number of cysteine residues, it is reinforced by multiple S–Au bonds [3].

The spontaneous adsorption of antibodies (Ab) onto the surface of citrate-capped AuNPs is a well-known process [4,5]. This antibody coating of the AuNPs exemplifies the so-called "protein corona," which spontaneously forms as soon as a nanoparticle enters a biological medium [6–8].

The protein corona on the surface of AuNPs imparts new characteristics to them, such as larger particle dimensions and different zeta potential. Furthermore, it provides steric hindrance to the AuNPs, reducing their aggregation and enhancing their stability even under conditions of high ionic strength. In fact, AuNPs tend to aggregate and precipitate at high ionic concentrations, but in the presence of the protein corona above a certain minimum concentration, nanoparticle-nanoparticle interactions are prevented.

It is important to note that inter-particle attraction due to van der Waals forces is substantial in the case of gold (due to its significant Hamaker constant). However, only with additional inter-particle repulsion can a dispersion of AuNPs remain stable [9]. In the case of citrate-capped AuNPs, the repulsive potential arises from electrical double layer (EDL) interactions associated with the negative charge of the citrate coating. The possible adsorption of large proteins, such as antibodies, introduces further steric stabilization. While pristine AuNPs precipitate at high electrolyte concentrations (as the repulsive EDL interaction diminishes at high ionic strength), the presence of a protein corona enables the nanoparticles to remain stable as a colloidal solution [1,10].

However, it should be considered that different proteins possess distinct properties that result in differences in their binding behavior with NPs.

In this paper, we present the surprising observation of an interaction between AuNPs and an antibody against L1 cell adhesion molecule (L1CAM), a glycoprotein involved in both neural and cancer development [11,12]. Under physiological pH and low ionic strength, this interaction leads to the formation of clusters of AuNPs coated by an Ab-corona, coexisting with large, micron-sized antibody aggregate structures. Strikingly, these aggregates disperse upon the addition of high NaCl concentrations, leaving the AuNPs surrounded by an Ab-corona. This behavior deserves thorough investigation as it underscores the importance of protein structure in the complexity of the protein-nanoparticle interaction.

2. Materials & Methods

2.1. Materials

Gold nanoparticles with a nominal diameter of 40 nm and a concentration of 1.5×10^{-10} M were purchased from BBI Solutions – UK. They have a z-average hydrodynamic diameter of 47 nm and a Zeta potential of -47 ± 2 mV. According to the manufacturer, the citrate content is below 0.04 % wt/vol.

The recombinant anti-L1CAM antibody Rabbit Monoclonal, hereafter referred to as αL1CAM, was purchased from Sino Biological Europe GmbH – Germany (catalogue number 10140-R001). It was obtained from a rabbit immunized with purified, recombinant Human L1CAM protein and stored in a 0.2 μm filtered solution in PBS at 1 mg/mL.

The recombinant anti-L1CAM antibody Mouse Monoclonal, referred to as mouse-αL1CAM, was used as a control in the experiments described in the Supporting Information. It was purchased from Sino Biological Europe GmbH – Germany (catalogue number 10140-MM01). It was obtained from a hybridoma resulting from the fusion of a mouse myeloma with B cells obtained from a mouse immunized with purified, recombinant Human L1CAM. It is also stored in a 0.2 μm filtered solution in PBS at 1 mg/mL.

The anti-CD63 mouse monoclonal antibody was purchased from Immunostep Salamanca-Spain (catalogue number 63PU) as a 1 mg/mL solution in PBS.

2.2. Light scattering

Dynamic Light Scattering (DLS) measurements were conducted in a microvolume quartz cuvette using a Zetasizer-NanoZS from Malvern. The instrument operated with a 4 mW He–Ne laser (633 nm wavelength) and a fixed detector angle of 173° (NIBS™). The instrument parameters (attenuator, optics position, and number of runs) were optimized by the instrument during data collection Typically, the time autocorrelation function (ACF) of scattered light intensity was obtained by averaging 12–16 consecutive runs, each lasting 10 s.

The ACF of scattered light intensity was then converted into the ACF of scattered electric field. This quantity represents the Laplace transform of the intensity-weighted size distribution function, which was determined using a standard regularized non-negative least squares analysis implemented by the manufacturer's software (Protein Analysis). The resulting intensity-weighted size distribution function provides information about the fraction of light intensity scattered by particles of different sizes.

To estimate the hydrodynamic size averaged over all particles in solution, the ACF of the electric field was fitted using a second-order cumulant expansion. This estimation is known as the z-averaged hydrodynamic diameter (dh), which emphasizes the contribution of the largest particles [13].

For static light scattering (SLS) experiments on antibody solutions, the intensity of light scattered by the sample (I), the filtered solvent only (I_{solv}) and the reference liquid toluene (I_{ref}) was measured using the same low-volume quartz cell. The data were then converted into absolute scattering intensities, referred to as "excess Rayleigh ratios" ($\Delta\Re$) as described by Ref. [14]:

$$\Delta\Re(\theta) = \frac{I - I_{solv}}{I_{ref}} \Delta\Re_{ref} \left(\frac{n}{n_{ref}}\right)^2$$

where $\Delta\Re ref = 14 \times 10^{-6}$ cm^{-1} is the Rayleigh ratio of toluene at 633 nm, n and n_{ref} are the refractive indices of the solution and toluene, respectively, at the same wavelength. For the calculation of n and subsequent calculations, it was assumed that the solution's refractive index increases by $(dn/dC) = 0.185$ cm^3/g (where C is the antibody weight concentration in g/mL).

2.3. Electrophoretic mobility

The electrophoretic mobility of AuNPs and antibodies was measured using Laser Doppler Electrophoresis (LDE) with the same Zetasizer-Nano ZS instrument used for DLS measurements. In these measurements, the scattered light was collected in forward scattering at a fixed detector angle of 17°. For gold nanoparticles, the zeta potential was subsequently determined from the electrophoretic mobility using the Smoluchowski approximation for spherical particles.

2.4. Morphological characterizations by transmission electron microscopy

TEM microscopy was conducted using an FEI Tecnai 12 instrument with the following specifications: high tension of 120 kV and a LaB6 filament. The AuNPs colloid suspension was dropped onto a Formvar®-coated Cu grid (400 mesh, Agar Scientific, Stansted, UK).

2.5. Visible spectroscopy

The extinction spectrum of AuNPs in the region between 400 and 950 nm was registered using an Agilent 8453 UV–vis diode-array spectrophotometer. Disposable plastic cuvettes were used for the measurements, and prior to the measurement, the sample volume was adjusted to 0.7 mL using the appropriate buffer.

2.6. Antibody titration of the AuNPs

The minimum antibody concentration required for the stabilization of AuNPs was determined using the protocol described in Ref. [15]. The samples were prepared directly in multiwell plates. Briefly, 20 μL of increasing antibody concentrations (ranging from 0.03 to 0.9 mg/mL) in 10 mM phosphate buffer (PB) at pH 7.4 were added to 250 μL of 40 nm AuNP suspensions at a concentration of 1.5×10^{-10} M. The mixtures of antibody-gold nanoparticles were allowed to equilibrate for 30 min, after which 100 μL of 1.85 M NaCl in 10 mM phosphate buffer was added to the samples. At this point, the samples contained increasing concentrations of antibodies and a fixed concentration of AuNPs at 1×10^{-10} M, in a solution of NaCl at 0.5 M and PB at 3 mM, with a pH of 7.4. If AuNP clusters were present, the solution colour turned purple/blue, whereas if the AuNPs were stabilized by a complete antibody corona, the solutions retained their original pink color. This protocol was used for AuNPs titration with all the antibodies (rabbit αL1CAM, mouse-αL1CAM, and αCD63).

To enable a fair comparison of the optical appearance of the samples containing the rabbit αL1CAM and AuNPs prepared under different ionic strength and mixing order conditions (further discussed in section 3.3), three sets of samples were prepared, all having the same final AuNP concentration (1×10^{-10} M), and a range of final αL1CAM concentrations from 0.0016 g/mL to 0.05 g/mL:

1) Control (without NaCl): 20 μL of increasing αL1CAM antibody concentrations (ranging from 0.03 to 0,9 mg/ml) in 10 mM PB at pH 7.4 were added to 250 μL of 40 nm AuNP suspensions at a concentration of 1.5×10^{-10} M. After 30 min, 100 μL of 10 mM PB at pH 7.4 were added to the samples. Under this condition, the AuNPs in the presence of αL1CAM aggregate.
2) 20 μL of the αL1CAM antibody (same concentrations as the control above) were first added to 100 μL of 1.85 M NaCl in 10 mM PB. The solution was then incubated for a sufficiently long time (5 h) to allow the proteins to adapt to this high ionic strength. Finally, 250 μL of AuNPs (1.5×10^{-10} M) were added to the samples.
3) 20 μL of the αL1CAM antibody (same concentrations as the control above) were first added to 250 μL of AuNPs (1.5×10^{-10} M) and incubated for 30 min. The situation is analogous to the control (the AuNPs aggregate) but with the AuNPs and antibodies 1.4 times more concentrated. The final concentration is then achieved by diluting the samples with 100 μL of 1.85 M NaCl in 10 mM PB.

3. Results

3.1. Phenomenology of rabbit αL1CAM-AuNP interactions

The improved colloidal stability of nanoparticles coated by a protein-corona is the basis of the preliminary step to form Ab-AuNP conjugates that can be exploited in several diagnostic tests [16]. In order to have good immunoactivity and performance tests it is important to avoid the presence of aggregates or poor conjugates. For example, aggregates can hinder the performance of paper-based immunoassay tests since big particles can block the pores of the membrane and avoid a correct flow of the analytes [17]. Therefore, previous to the nanoparticle conjugation with an Ab, it is important to find the minimum concentration that stabilizes the NPs and prevents aggregate formation. To accomplish this, the AuNPs are first incubated in a low ionic strength buffer with increasing Ab concentrations. Under these conditions, repulsive electrostatic double-layer (EDL) interactions stabilize the colloidal gold sol, retaining its pink-orange color, while spontaneous adsorption of Abs onto the nanoparticle's surface takes place. Subsequently, a concentrated NaCl solution is added, fully screening any EDL stabilization and inducing the aggregation of uncoated AuNP. This is visibly evident as the solution's color changes to purple or blue (depending on the size of the clusters), eventually resulting in the precipitation of the AuNPs. On the contrary, when there is a sufficient amount of Ab to form a complete coverage of the AuNPs, no change in color is observed due to the steric repulsion provided by the Ab corona, which stabilizes the colloidal sol. The minimum concentration required to form a complete protein corona corresponds to the lowest Ab concentration at which the AuNP solution does not change color upon high NaCl loading [4,15]. This phenomenon is well-established and has been confirmed with various antibodies worldwide [16]. Recently, we utilized gold nanoparticles for labeling αL1CAM. We performed the aforementioned titration in a low ionic strength buffer. Surprisingly, the outcome of the bioconjugation differed from our expectations. As soon as we added the αL1CAM to the AuNPs, the solution turned purple in all the tested Ab concentrations, as depicted in Fig. 1A, retaining the pink-orange color only in the first well where the Ab was absent.

The purple color of the AuNPs indicates the formation of large aggregates upon the addition of this antibody. This is further confirmed by the significant changes in the extinction spectra of the AuNPs observed shortly after mixing the solutions (Fig. 1B). The original single nanoparticle plasmon resonance at 526 nm, characteristic of monodispersed AuNPs, gradually diminishes in intensity, while a new plasmon band emerges at 610 nm, indicative of the formation of clusters comprising closely spaced AuNPs. This shift in the extinction spectra can be utilized as a quantitative "index of aggregation," calculated by dividing the extinction at 610 nm by that at 526 nm ($R_{610/526}$). The dependence of $R_{610/526}$ on the Ab concentration is shown in Fig. 2A. When [Ab] $\leq$ 0.025 mg/mL, $R_{610/526}$ is approximately 0.07, indicating dispersed AuNPs. However, at higher concentrations $R_{610/526}$ exhibits a steep increase, saturating at $R_{610/526}$–1.2 for [Ab]>0.15 mg/mL.

The samples in Fig. 1A were also analyzed using Dynamic Light Scattering (DLS). Fig. 2B shows the relationship between the mean hydrodynamic diameter (evaluated as z-average by cumulant analysis of the ACF) and the Ab concentration. Pristine AuNPs have a d_h of 47 nm, and the addition of Ab at concentrations $\leq$0.025 mg/mL has no impact on the observed size. However, for Ab concentrations above 0.025 mg/mL, a dramatic increase in the size of the particles in solution is observed. The measured d_h increases to 150 nm at [αL1CAM] = 0.05 mg/mL and reaches values of around 800 nm for [αL1CAM] > 0.15 mg/mL.

The trend in size observed in Fig. 2B is parallel to the dependence of $R_{610/526}$ on the Ab concentration, as shown in Fig. 2A However, it is important to note that the aggregates present in the solution cannot be solely attributed to AuNPs. While a surface plasmon resonance peak around 600 nm would indicate the presence of small AuNP clusters, the existence of micron-sized aggregates would lead to a featureless extinction covering the entire wavelength range from 600 nm to the NIR.

A reliable method to assess the aggregation of AuNPs and/or antibodies is by examining the intensity size distribution function (SDF). This function represents the fraction of light scattered by particles of various hydrodynamic sizes, which can be derived from the field autocorrelation function (ACF) obtained during a DLS measurement. Fig. 1C displays representative intensity size distributions. The pristine AuNPs exhibit a narrow diameter distribution centered around 47 nm. However, upon introducing 0.36 mg/mL αL1CAM into the sample, the distribution of the Ab-AuNP mixture shifts towards significantly larger sizes, reaching values of 1 μm or greater. It is important to note that the calculated SDF for the Ab-AuNP mixture underestimates the particle sizes, as the numerical procedure used to extract the SDF from the experimental ACF neglects the contribution from particles larger than 1 μm. Consequently, the particles present in the Ab-AuNP mixture are larger than 1 μm. Their presence is clearly demonstrated in the field autocorrelation function depicted in Fig. S1, where a distinct slow component is observed. This slow component does not decay for correlation times exceeding 2 ms. DLS analysis of αL1CAM in the absence of AuNPs indicates that some of the antibodies are aggregated The SDF in Fig. 1C shows a peak at a hydrodynamic diameter (d_h) of 12 nm, likely corresponding to monomeric Ab, along with aggregates of dh 40 nm and even 200 nm. The self-aggregation properties of this αL1CAM antibody are discussed in detail

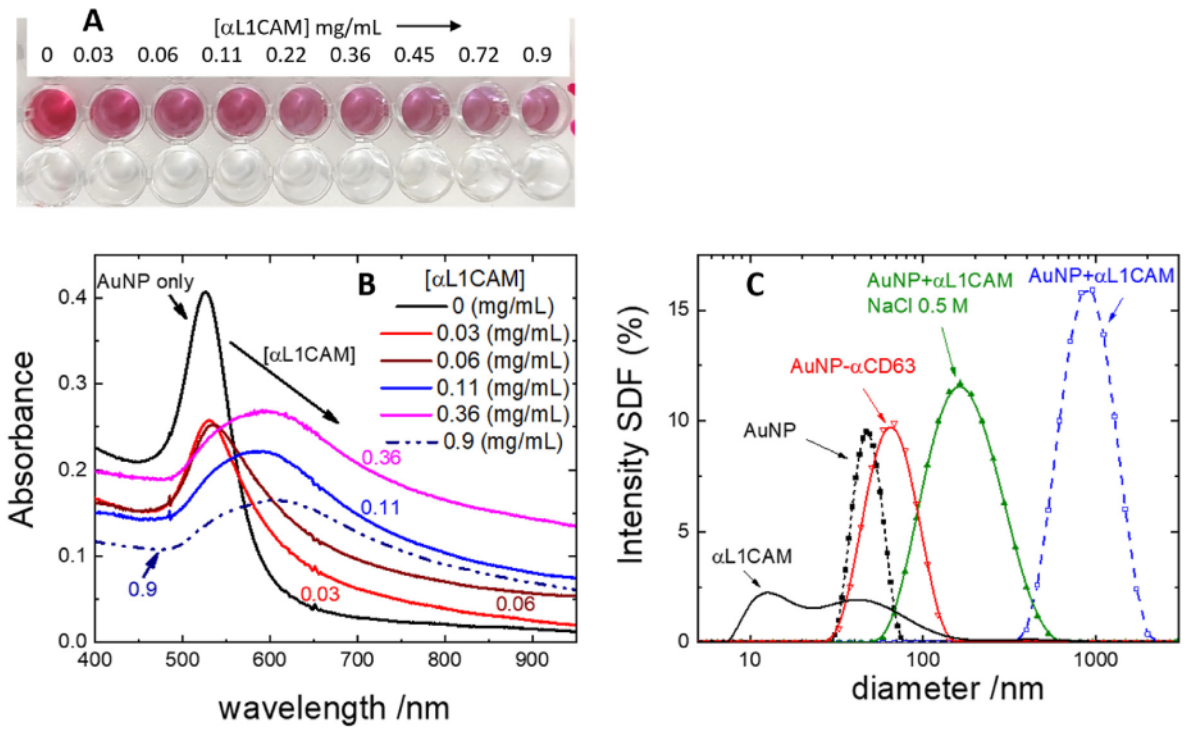

Fig. 1. - AuNPs aggregation in presence of αL1CAM (concentrations refer to the initial 20 μL Ab solution see section 2 for details): A) picture of the samples at [AuNP] = 0.14 nM and increasing concentrations of Ab at low ionic strength. B) AuNPs absorption spectra for some representative samples shown in panel A after dilution to 0.7 mL. Conditions in cuvette: 10 mM Phosphate Buffer, pH = 7.4; [AuNPs] = 0.05 nM. C) Intensity size distribution functions performed on different samples. Conditions: 10 mM Phosphate Buffer, pH = 7.4, when indicated NaCl to a final concentration of 0.5 M was added to PB; [AuNPs] = 0.1 nM, [αL1CAM] = 0.36 mg/mL.

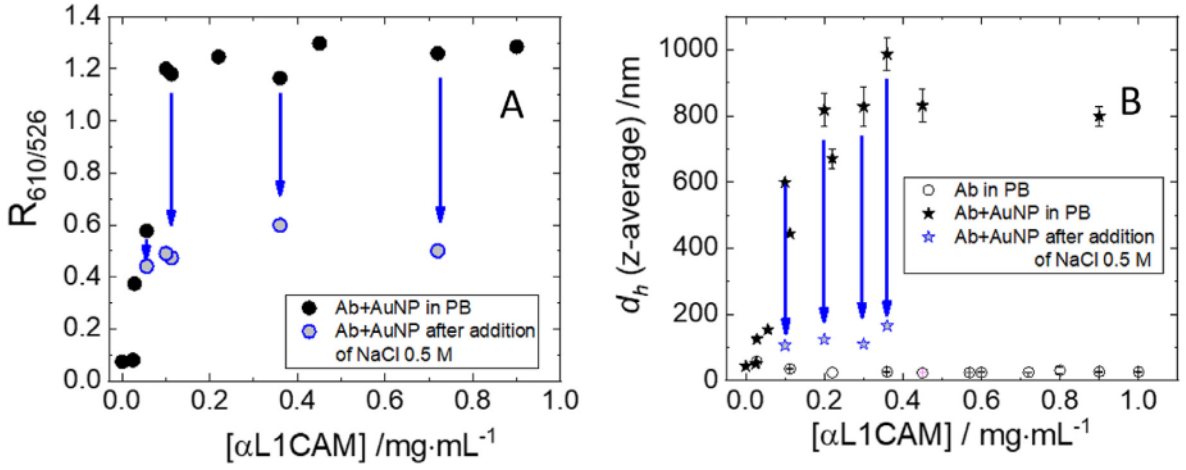

Fig. 2. - αL1CAM-AuNPs conjugates characterization in different conditions of ionic strength and increasing concentrations of Ab: A) AuNPs aggregation index (R is the Ratio of absorptions measured at 610 and 526 nm), measured on the same samples. Conditions: 10 mM Phosphate Buffer, pH = 7.4, when indicated NaCl to a final concentration of 0.5 M was added to PB; [AuNPs] = 0.1 nM. B) z-average hydrodynamic diameter measured by means of DLS: black stars represent AuNPs in presence of different concentration of Ab in 10 mM Phosphate Buffer, pH = 7.4; grey stars are data after addition of salt to a final concentration [NaCl] = 0.5 M; open circles are the sizes of the antibody alone.

in a dedicated section. Here, we want to emphasize that the large micrometer-sized aggregates observed in the Ab-AuNP mixture are not present in the pristine Ab. Furthermore, since the pristine AuNPs scatter light significantly more than the pristine Ab, the DLS measurement of the mixture primarily captures the Brownian motion of the (aggregated) nanoparticles.

To investigate this further, we conducted analysis using TEM. Representative TEM micrographs are presented in Fig. 3. At low ionic strength, clusters consisting of 20–60 spherical AuNPs are clearly visible as dark spots (Fig. 3A). These small clusters contribute to the distinct plasmon resonance extinction peak observed at 610 nm (Fig. 1B). At higher magnification, TEM micrographs reveal a thin, low-contrast layer surrounding the AuNP clusters, attributable to the organic matter of the antibodies. Interestingly, this low-contrast matter appears to be directly connected to very large particles, which are identified as significant Ab aggregates. The size of these aggregates corresponds to the micrometer-scale hydrodynamic radii probed by DLS.

By combining the information gathered from the extinction spectra, DLS, and TEM analyses, we can deduce that the addition of αL1CAM to citrate-capped AuNPs at low ionic strength and physiological pH leads to

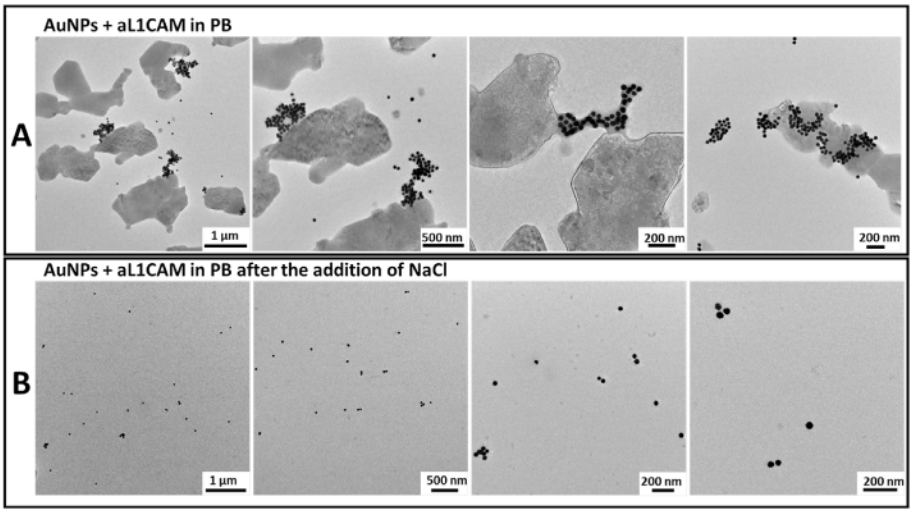

Fig. 3. - TEM micrographs of αL1CAM-AuNPs conjugates at different magnifications ([AuNPs] = 0.15 nM, [αL1CAM] = 0.25 mg/mL, in 10 mM Phosphate Buffer, pH = 7.5) before (A) and after (B) addition of NaCl (final concentration of 75 mM).

two effects: the aggregation of antibodies and the formation of clusters consisting of AuNPs coated with Ab. Notably, the AuNP clusters are composed of a limited number of NPs, indicating that the coagulation of AuNPs is not infinite. Additionally, these AuNP clusters are associated with micron-sized Ab aggregates, resulting in shared hydrodynamic sizes.

These characteristics are specific to the recombinant α-L1CAM Antibody (IgG), derived from a *rabbit* immunized with purified recombinant Human L1CAM, and are highly reproducible across different purification batches. It is important to mention that an analogous antibody obtained from the same manufacturer using mouse tissue immunized with the same antigen (refer to the mouse-αL1CAM details in the Materials & Methods section) does not induce aggregation. Instead, it forms a protective corona at low ionic strength, as described in the "Additional Experiments on mouse-αL1CAM" section of the Supporting Information.

3.2. *Interlude: a survey of century-old papers*

In the attempt to comprehend the peculiar behavior of the αL1CAM obtained from rabbit when exposed to AuNPs we embarked on a literature survey The aggregation of AuNPs induced by Ab is relatively uncommon, and we discovered only a recent article by Okyem et al. that reports how, under acidic conditions (pH $\leq$ 7.0), IgG triggers the aggregation of AuNPs [18]. The authors propose that the bridging of the antibody to the negatively charged AuNPs is the primary mechanism behind this aggregation phenomenon. They explain that at acidic pH, the antibody forms positively charged patches, while at physiological pH, IgG assumes the conventional corona structure, stabilizing the AuNPs. Their study does not mention any self-aggregation of the antibodies, and the featureless plasmon observed in the red region of the AuNPs' extinction spectra aligns with the large sizes detected by DLS (hundreds of nanometers). The recent literature on AuNP aggregation induced by proteins (different from antibodies) is relatively limited, although a review article (see Ref. [19]) covers this topic in more detail. It highlights the coexistence of protein-AuNPs assemblies alongside large protein aggregates without embedded nanoparticles, particularly for positively charged proteins such as Lysozyme and Avidin. These phenomena are attributed to electrostatic attractions between proteins and AuNPs, leading to the unfolding of proteins and subsequent formation of amorphous NP-free protein aggregates [20,21].

Interestingly, during our exploration, we encountered a series of papers published between 1900 and 1930 that addressed this subject. This finding was both surprising and inspiring for the subsequent experiments detailed in the following section. Consequently, we believe it would be valuable to provide a brief review of these historical papers.

In retrospect, the existence of old papers examining protein-AuNPs interactions is not surprising, as the history of gold colloids (referred to as AuNPs in modern terminology) is closely intertwined with their interactions with biological matter. As early as 1898 Zsigmondy (Nobel's laureate in 1925 for his work on the nature of colloids) reported that solutions of proteins protect a colloidal gold solution from precipitation [22]. This was one of the first hints of the formation of protein corona around nanoparticles.

Of particular relevance to our investigation, and fundamental in the history of neurological laboratory diagnostics, is the so-called Lange's *colloidal gold reaction*. In 1912, Lange observed that colloidal gold remains stable in 0.4% NaCl (~7 mM) but precipitates upon addition of cerebrospinal fluid (CSF) from patients with certain pathologies [23,24]. Moreover, the extent of gold precipitation as a function of the dilution of CSF was related to the pathology, so that the *colloidal gold reaction* was the standard clinical test to discriminate between multiple sclerosis, neurosyphilis and meningitis up to the advent of protein electrophoresis in the 1940's. To perform such a test [25] CSF samples were serially diluted with 0.4% NaCl in 10 test tubes, ranging from 1/10 to 1/5120 in volume. A fixed amount of AuNPs was then added, and a numerical score was assigned based on the optical appearance of the tubes after 12 h. The score ranged from 0 (no change in color) to 5 (complete gold precipitation). The optical appearances and corresponding scores are depicted schematically in Fig. S2A in the Supporting Information. Lange suggested representing the precipitation outcomes with three distinct curves, namely the paretic, luetic (or tabetic), and meningeal curves, as illustrated in Fig. S2B. The luetic curve indicated gold nanoparticle precipitation at intermediate dilution and was indicative of neurosyphilis, while the paretic curve signified gold coagulation in the early tubes but not at very high dilution, associated with what is now known as multiple sclerosis. Non-syphilitic meningitis, on the other hand, displayed gold precipitation only at very high dilution. In clinical practice, the test results were condensed into a single aggregate figure, such as 5555400000, indicating precipitation in the first five tubes, and so forth. In 1922, meticulous investigations by Cruickshank [27] demonstrated that "*The substance in the spinal fluid of general paralytics which causes precipitation of colloidal gold is not dialysable, and resides in the globulin fraction of the protein*". Subsequently, the advent of protein electrophoresis clarified that the colloidal gold reaction activity was associated with the gamma globulin fraction (i.e., antibodies) in spinal fluid [26,27]. However, modern techniques of protein analysis, which could have shed more light

on the phenomenon, rendered Lange's test obsolete, and it has since fallen, definitively, into oblivion. Regarding the phenomenology discussed in the previous section, the 1922 paper by Cruickshank [27] contains two important pieces of information:

- The author demonstrates that "*As the globulins obtained from negative spinal fluids, even when used in concentrated form, are almost inactive, the precipitating action of paretic fluids cannot be ascribed solely to the increase in globulin but is probably dependent on a specific alteration of the physical state of the globulin, which is associated with a positive electric charge*". In other words, the reaction is specific for certain antibodies and not applicable to all antibodies, which agrees with our experimental observations regarding the coagulation of AuNP at low ionic strength only in the case of αL1CAM from rabbit.

- The dependence of the colloidal gold reaction on the salinity of the medium has been investigated, yielding counterintuitive results. "*Spinal fluids which are active in precipitating colloidal gold under the conditions of Lange's test also possess protective power under other conditions, …. If to a series of tubes, each containing 0.*15 c.c. *of 10 per cent. NaCl solution, graded amounts of a paretic fluid are added it will be found on adding 2.*5 c.c. *of colloidal gold to each tube that the tubes with large amounts of spinal fluid show no precipitation, while the tubes with insufficient fluid show the colour change and precipitation produced by this amount of salt*". In other words, if the test is performed at high ionic strength, the classical scenario observed in customary "protein titration" is observed: AuNPs remain stable at high protein loading, while incomplete corona formation (low protein loading) leads to coagulation of the nanoparticles.

3.3. Effect of the ionic strength on the rabbit αL1CAM-AuNP interactions

Inspired by Cruickshank's 1922 paper, we investigated the effect of increased ionic strength on the aggregates formed by αL1CAM and AuNPs (reader is referred to the Materials and Methods section for details). The antibody was diluted in 10 mM PB (pH 7.4) containing 0.5 M NaCl and allowed to equilibrate for 5 h before adding the AuNPs (lane 2 in Fig. 4A). As a control, a parallel set of samples was prepared using PB without NaCl as the diluent (lane 1 in Fig. 4A). At low ionic strength (lane 1), the presence of the antibody led to coagulation of AuNPs regardless of the antibody concentration. However, at 0.5 M NaCl, coagulation was prevented when the antibody concentration was sufficiently high ([Ab] $\geq$ 0.3 mg/ml in the initial 20 μL), and the solutions exhibited the characteristic orange-pink color of dispersed AuNPs (lane 2). Thus, it appears that at high ionic strength and with a sufficiently high antibody concentration, the antibodies form a protective corona on the nanoparticle surface, preventing AuNP coagulation. In this experiment, AuNPs were added to a solution of antibodies at high ionic strength. Since coagulation of AuNPs occurs promptly in the presence of only 0.5 M NaCl, the antibodies must adsorb onto the nanoparticle surface before irreversible aggregation takes place. To separate the kinetic aspects from the thermodynamic affinity of the antibodies for the AuNPs, we conducted an experiment with a different mixing order. The αL1CAM and AuNPs were mixed and incubated for 1 h. Up to this step, the protocol was identical to that described in section 3.1, and indeed, all solutions containing antibodies changed color due to the formation of the previously mentioned AuNP clusters. Subsequently, a concentrated NaCl solution was added to each well, raising the ionic strength to 0.5 M. At this high ionic strength, all solutions containing αL1CAM reverted back to the orange-pink color, as shown in Fig. 4A, lane 3. A comparison of the results from lanes 1 and 3 of Fig. 4 indicates that the αL1CAM-induced clustering of AuNPs is reversed at high ionic strength. However, high salinity is a condition that typically induces AuNP aggregation unless they are shielded by a protective protein corona. In this regard, the comparison between the results from lanes 2 and 3 of Fig. 4 suggests that when AuNPs are simultaneously exposed to high salt content and antibodies, they are stabilized only if the antibodies adsorb onto the nanoparticle surface faster than salt-induced NP-NP aggregation. Since the rate of adsorption is proportional to the antibody concentration, this occurs only when the αL1CAM content is sufficiently high (experiments in lane 2 of Fig. 4). On the other hand, a very small amount of antibody is enough to form a protein corona on the nanoparticles over a long timescale (i.e., when the AuNPs are first incubated with the antibodies), as demonstrated in the experiments of lane 3 of Fig. 4.

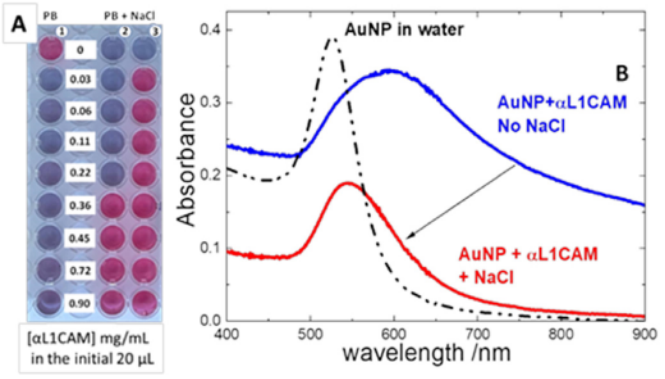

Fig. 4. - AuNPs aggregation in presence of increasing concentrations of αL1CAM and in different conditions of ionic strength.
A) picture of the samples obtained with a different NaCl addition sequence: lane 1) control without NaCl: 20 μL of increasing αL1CAM antibody concentrations (from 0.03 to 0,9 mg/ml) in 10 mM PB pH 7.4 + 250 μL of AuNP 1.5×10^{-10} M 100 μL of PB 10 mM pH 7.4; lane 2) 20 μL of the αL1CAM antibody at same concentrations of lane 1 incubated first with 100 μL of 1.85 M NaCl in 10 mM PB and subsequent addition of 250 μL of AuNP 1.5×10^{-10} M; lane 3) 20 μL of the αL1CAM antibody (same concentrations of lane 1) first incubated with 250 μL of 1.5×10^{-10} M AuNP and subsequent addition of 100 μL of 1.85 M NaCl in 10 mM PB.
B) AuNPs representative extinction spectra of samples prepared with 20 μL [Ab] = 0.45 mg/ml (third wells from the bottom in panel A) with (lane 3) and without salt (lane 1); samples have been diluted to 0.7 mL with the suitable buffer. As a reference the spectrum of AuNP in water is also shown.

Representative extinction spectra of AuNP are shown in Fig. 4B. The low ionic strength solution is characterized by a broad plasmon centered at 610 nm and a long wavelength tail. After the increase in salinity, the plasmonic peak narrows and undergoes a blue shift. At NaCl 0.5 M, the position of the extinction maximum is 546 nm, suggesting the presence of a slight degree of clustering. Accordingly, the aggregation parameter $R_{610/526}$ does not drop to the value of 0.07 observed for pristine AuNP but instead decreases from $R_{610/526}$–1.2 to $R_{610/526}$–0.5 regardless of the concentration of αL1CAM (see Fig. 2A). Additionally, the hydrodynamic size measured by DLS exhibits a significant decrease following the increase in salinity. Fig. 1C compares the SDFs measured before and after the addition of NaCl. It is evident that a NaCl concentration of 0.5 M is sufficient to disaggregate the micron-sized particles, resulting in objects with a diameter of approximately 150 nm. The SDF at high ionic strength is broad, and its mean (z-average) diameter remains independent of αL1CAM concentration (as shown in Fig. 2B). For comparison, Fig. 1C also includes the SDF of pristine AuNPs and the SDF of AuNPs conjugated with the antibody against tetraspanin CD63, which forms a protein corona in a predictable manner. Upon coating with αCD63, the diameter of AuNPs increases from 46 nm to 64 nm, consistent with an antibody layer thickness of approximately 9 nm. These results are in line with previous data (see Ref. [28]). The nearly twofold increase in size observed in the case of AuNPs plus αL1CAM at high salinity, along with the broadness of the SDF, suggests the coexistence of AuNP oligomers with isolated nanoparticles. This deduction was confirmed by TEM micrographs taken of a solution of AuNPs and αL1CAM at high ionic strength. To minimize the presence of NaCl crystals on the TEM grids, the ionic strength for these experiments was maintained at 75 mM, which was still sufficient to produce a pink color in the solutions. As shown in Fig. 3B, at high ionic strength, the AuNPs are predominantly present as isolated particles or dimers/trimers. Furthermore, the micrographs

reveal that the micron-sized protein aggregates, prevalent at low ionic strength, have been dissolved by the increase in NaCl concentration (compare Fig. 3A and B).

All the above-described results have been obtained within 5 months from the purchase of αL1CAM. Within this time frame, αL1CAM stored at 8 °C consistently provided reproducible results (we tested different batches). However, for longer storage periods, the antibody begins to aggregate. The SDF of αL1CAM stored for 8 months at 8 °C and then redissolved in PB is presented in Fig. S5. The SDF exhibits a monomodal peak (z-average diameter of 850 nm with a width of 380 nm). At this level of aggregation, αL1CAM does not induce clustering of AuNPs (the gold solution does not change color upon Ab loading). Interestingly, the addition of NaCl to the mixture of AuNPs and aggregated αL1CAM does not induce AuNPs aggregation. Indeed, the extinction spectra of AuNPs are typical of non-aggregated AuNPs with a $R_{610/526}$ <0.4 (data not shown) suggesting that the antibody has lost its destabilizing effect at low ionic strength but still maintains its protective properties at high ionic strength. Notably, the SDFs obtained in the case of AuNPs and aggregated αL1CAM in NaCl 0.5 M (Fig. S5 in the Supporting Information) exhibit a peak at $d_h = 72$ nm (width 32 nm) closely resembling the peak reported in Fig. 1C for AuNP stabilized by a complete corona of the "well behaving" antibody (αCD63). In passing, this confirms that in the DLS experiments conducted in the presence of AuNPs, we are only measuring the Brownian motion of the metallic particles, thereby obscuring the contribution of protein aggregates.

3.4. αL1CAM self-aggregation

The evidence that αL1CAM induces precipitation of AuNP at low salinity but stabilizes the solution at high salinity is somewhat counter-intuitive. The behavior of pristine citrate-capped AuNPs is the opposite, as they are stable at low salt content but precipitate at high salinity. Therefore, the underlying cause of this unusual behavior should be attributed to the colloidal stability of αL1CAM itself. To investigate this, the electrophoretic mobility of αL1CAM alone in NaCl-free phosphate buffer (10 mM) was determined using Laser Doppler Electrophoresis (LDE), resulting in a value of $(-0.70 \pm 0.05)\text{x}10^{-4}$ cm^2/Vs This indicates that at pH 7.4, the antibody carries an overall negative charge, as it is above its isoelectric point. In solutions containing NaCl 0.5 M, the electrophoretic mobility decreased to $(-0.13 \pm 0.03)\text{x}10^{-4}$ cm^2/Vs due to the screening effect of the electrolyte on the antibody charge.

In addition to the fast aggregation observed in the presence of the AuNPs, αL1CAM also undergoes slow self-assembly over a period of more than five months at the storage temperature. To gain further insight into the nature of the antibody's self-interactions, the molecular weight and the 2nd virial coefficient of αL1CAM dissolved in PB (10 mM pH 7.4) with and without NaCl 0.5 M were measured using static light scattering (SLS). The intensity of the scattered light was converted into absolute scattering intensities, i.e. "excess Rayleigh ratios, Δℜ, " as described in the experimental section. Since the antibody molecules are much smaller than the wavelength of the light, the intensity values measured at a scattering angle of 173° were directly used (i.e. Δℜ(173°)~Δℜ(0)). In addition, the aggregates present in the 8 months old αL1CAM solutions were also examined. For non-ideal solutions of small particles, the dependence of the Δℜ on the ponderal concentration C (g/mL) is described by the Debye's equation:

$$\frac{K_{opt}C}{\Delta\Re} = \frac{1}{Mw^{app}} + 2B_2C$$

Where $K_{opt} = \frac{4\pi^2 n^2 \left(\frac{dn}{dC}\right)^2}{N_a \lambda^4}$, n is the refractive index of the solution, $dn/dC = 0.185$ mL/g is the refractive index increment of the antibodies, N_a is the Avogadro's number, λ is the wavelength of the laser in vacuum, Mw^{app} is the average molecular weight, and B_2 is the second virial coefficient. Attractive interactions present values $B_2 < 0$ while repulsive interactions are characterized by $B_2 > 0$.

The Debye plots ($K_{opt}C/\Delta\Re$ vs. C) of freshly purified αL1CAM at high and low ionic strengths are shown in Fig. 5A. In the case of the αL1CAM dissolved in PB at low ionic strength, the $K_{opt}C/\Delta\Re$ values decrease with increasing Ab concentration. This evidences a negative 2nd virial coefficient ($B_2 = (-1.2 \pm 0.5)\text{x}10^{-4}$ mol mL/g^2) suggesting attractive interactions between antibodies at low salinity. This observation is consistent with the slow self-assembly that takes place during long storage times.

The analogous evaluation of the αL1CAM in solutions at high ionic strength yields remarkable results. The increase in salinity results in a positive 2nd virial coefficient ($B_2 = (+3.6 \pm 1)\text{x}10^{-4}$ mol mL/g^2), indicating the presence of repulsive forces between the Abs. This finding emphasizes the electrostatic nature (EDL) of these interactions In colloids with a uniform charge distribution, the EDL interaction is typically repulsive and is screened by a sufficiently high ionic strength. However, in the case of αL1CAM, we observe the opposite behavior. This can be explained by assuming a non-uniform charge distribution, such as a patchy model for antibody molecules [29–32], where different patches carry opposite charges, leading to attraction between positive and negative patches on different antibodies. However, an increase in ionic strength will screen these interactions, eliminating the attraction and leaving only the repulsive excluded volume interaction.

The corresponding molecular weights, evaluated as the reciprocal of the intercept of the regression line according to Debye's equation, are similar in PB and in PB + NaCl, being 4.3×10^5 g/mol and 5.6×10^5 g/mol, respectively. These estimates are about three to four times larger than the molecular weight of a typical antibody. However, since the DLS (Fig. 1C) reveals the presence of aggregates in the solution, these values should be considered as an apparent molecular weight, accounting for the coexistence of monomers and already formed oligomers.

In the same experiments, the hydrodynamic diameters were determined by DLS and are presented in Fig. 5B. The d_h-values do not show any concentration dependence, and the size ($d_h = 25 \pm 2$ nm) remains consistent within the experimental error, regardless of the ionic strength.

Upon prolonged storage at 8 °C, the αL1CAM undergoes self-

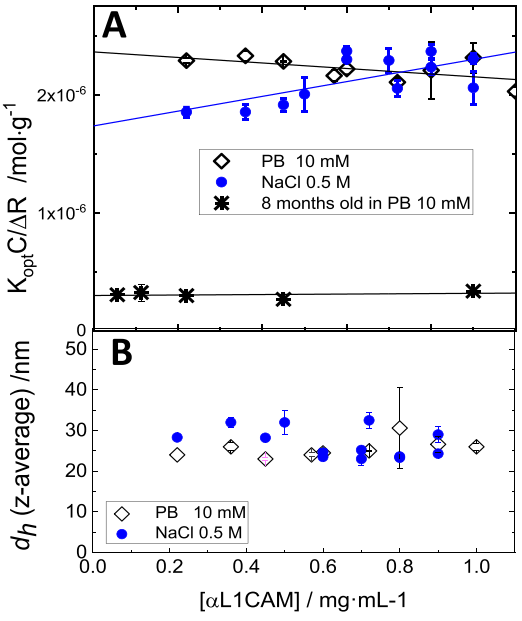

Fig. 5. αL1CAM self-aggregation. **A)** Debye's plot of (freshly purified) αL1CAM at high (full circle) and low (open diamond) ionic strengths; also shown are the data for Ab stored for 8 months at 8 °C (asterisk). **B)** hydrodynamic diameters of samples in A) determined by means of DLS.

assembly, forming large aggregates with size of $d_h = 850 \pm 50$ nm. Diluting these aggregates with both PB 10 mM and PB + NaCl 0.5 M does not alter their size (data not shown). The dependence on the scattered light upon dilution is the same, within the experimental error, regardless of the ionic strength of the diluent. The corresponding Debye plot is also displayed in Fig. 5A (for the sake of readability, only the data on PB are shown) indicating very weak repulsive interactions ($B_2 = (+2 \pm 4)x10^{-5}$) and a substantial molecular weight of $(3.3 \pm 0.3)x10^7$ g/mol corresponding to ~220 IgG molecules.

4. Discussion

At low ionic strength, the addition of citrate-capped AuNPs to αL1CAM, purified from rabbit, induces the sudden aggregation of the antibodies, forming NP-free aggregates and causing clustering of AuNPs with an Ab corona (Figs. 1–3). However, increasing the ionic strength to 0.5 M eliminates Ab self-aggregation and dissolves almost all AuNP clusters, leaving only a few dimers present, while the stabilizing Ab corona remains intact on the surface of the AuNPs (see Figs. 1 and 3). These observations indicate that Ab self-aggregation is driven by attractive electrostatic double-layer (EDL) forces, whereas the formation of an Ab corona on AuNPs depends on the chemical affinity of the Ab for the gold surface. At physiological pH (7.4), which is above αL1CAM's isoelectric point (as evidenced by the negative electrophoretic mobility), the antibody carries an overall negative charge. Thus, the electrostatic attraction between Abs may be attributed to the presence of oppositely charged patches on different regions of the molecule, as suggested for other antibodies [31–34]. The chemisorption of Abs onto the AuNPs is likely facilitated by the large number of cysteine residues on their structure [33,34]. In agreement with these findings, in the absence of AuNPs, αL1CAM self-interactions are attractive ($B_2 < 0$) at low ionic strength, leading to very slow self-aggregation. However, the interactions become repulsive ($B_2 > 0$) at high ionic strength.

In light of these observations, it appears that the presence of AuNPs enhances Ab-Ab interactions. At low salinity, where Abs attract each other, the presence of AuNPs promotes their aggregation. Furthermore, when two Ab-coated AuNPs collide, they remain attached due to the attraction between Abs on different particles (refer to the low ionic strength pathway in Fig. 6). However, as the Ab-Ab interactions become repulsive with increasing ionic strength, the Ab aggregates dissolve, and the Ab-coated AuNPs repel each other (refer to the high ionic strength pathway in Fig. 6).

The mechanism by which AuNPs accelerate antibody self-aggregation is currently unknown. The AuNP-induced aggregation of positively charged proteins (such as lysozyme and avidin) has been previously explained in terms of partial unfolding of the protein adsorbed on the gold surface, which promotes further protein aggregation [22]. However, the effect of nanoparticles can also be understood in terms of a kinetic mechanism. In the absence of AuNPs and at low ionic strength, Abs self-aggregate slowly during storage (at 8 °C and a concentration of 1 mg/mL). Considering the spontaneous binding of Abs to AuNPs through the favorable reaction between the thiols of cysteine residues and the gold surface, the presence of AuNPs is expected to increase the rate of Ab-Ab self-assembly.

Reaction-controlled bimolecular processes are characterized by a negative entropy penalty because the two reactants need to restrict their motion and align correctly for the reaction to occur. This implies a negative contribution to translational, rotational, and vibrational entropy upon binding. However, when reactants are immobilized on a solid surface through favorable adsorption, the entropic penalty has already been paid upon binding, allowing for a smaller entropy loss and overcoming the activation barrier. In enzymology, the binding of substrate to an enzyme brings reacting groups into close proximity, resulting in the so-called Jencks's Circe effect [35]. In fact, experiments involving immobilization of odorant binding proteins on gold surfaces through thiol chemistry have demonstrated that substrate-protein binding

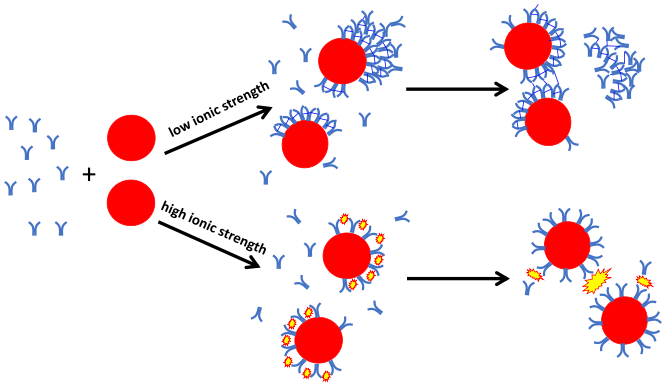

Fig. 6. - Cartoon showing the Ab-Ab and the AuNP-Ab interactions in different conditions of ionic strength. The explosions represent repulsive interactions while the connecting lines attractive interactions.

constants are at least three orders of magnitude larger than those measured in solution [36]. In the case of antibody immobilization on AuNPs at low salinity, we expect an even greater increase in Ab-Ab affinity since both reactants (two Ab molecules undergoing self-assembly) are immobilized. Furthermore, in addition to the thermodynamic advantage, a kinetic effect is also expected. When two antibodies are immobilized in close contact, they cannot move away and can rapidly find the required mutual orientation for dimerization.

Once a corona composed of Abs bound to each other is formed, the strong Van der Waals attraction between AuNPs promotes nanoparticle contact, leading to the formation of clusters linked by attractive Ab-Ab interactions. Eventually, the large size of these clusters enhances the incorporation of further antibodies. The relative collision rate between a cluster and a monomeric Ab can be described by $k_d = 4\pi(r_{cluster} + r_{Ab})(D_{cluster} + D_{Ab})$, where r_i and D_i are the size and diffusion coefficient of the reactant I [37]. For large enough clusters ($r_{cluster} \gg r_{Ab}$ and $D_{cluster} \ll D_{Ab}$) this equation simplifies to $k_d = \frac{2}{3} r_{cluster}/r_{Ab}$. Therefore, the collision rate between an Ab monomer and clusters consisting of AuNPs and antibodies increases linearly with the cluster size. This scenario holds as long as Ab-Ab interactions remain attractive. However, when a sudden increase in ionic strength turns these interactions repulsive, all aggregates are disrupted, and only individual Ab-coated nanoparticles remain in solution. The repulsion between Abs ensures the stability of these particles.

5. Conclusions

Citrate-capped AuNPs are monodisperse in phosphate buffer (10 mM pH 7.4) but the addition of rabbit monoclonal antibodies against L1CAM protein induces their immediate coagulation. Interestingly, the coagulation can be completely reversed by adding NaCl to a final concentration of 0.5 M. This behavior is specific to the αL1CAM antibody from rabbits and is not observed with the same antibody purified from mice.

The combination of extinction spectra, DLS, and TEM measurements unequivocally demonstrates that the coexistence of AuNP with αL1CAM, at low ionic strength, induces the formation of micron-sized antibody aggregates and smaller clusters of AuNPs coated by the antibodies. SLS measurements confirm that αL1CAM exhibits attractive self-interactions at low ionic strength and undergoes extremely slow aggregation over time. Based on these findings, we propose that the presence AuNPs speeds-up this aggregation process, as the entropic penalty associated with Ab-Ab aggregation has already been paid upon the highly favorable binding of the Abs to the gold surface. Additionally, the high concentration of Abs in the protein corona around the AuNP promotes Ab-Ab aggregation. In agreement with this, at high ionic strength where SLS reveals repulsive interactions between antibodies, the Ab aggregates dissolve, resulting in a solution containing only monomeric antibodies

and isolated AuNPs coated with an antibody corona.

This unusual behavior may have been overlooked or mistakenly attributed to errors in bioconjugation protocols. With this study, we aim to shed light on the complexity of antibody-nanoparticle interactions.

Declaration of competing interest

The authors declare that they have no known competing financial interests or personal relationships that could have appeared to influence the work reported in this paper.

Data availability

Data will be made available on request.

Acknowledgments

Dr. Maria Liguori is kindly acknowledged useful discussion. H.M. was funded by POR PUGLIA FESR-FSE 2014/2020 Research for Innovation (REFIN)-Codice Pratica: 7BDC8679.

Appendix A. Supplementary data

Supplementary data to this article can be found online at https://doi.org/10.1016/j.jciso.2023.100089.

References

[1] Y. Yu, Y. Luan, W. Dai, Dynamic process, mechanisms, influencing factors and study methods of protein corona formation, Int. J. Biol. Macromol. 205 (2022) 731–739, https://doi.org/10.1016/J.IJBIOMAC.2022.03.105.
[2] W. Lin, T. Insley, M.D. Tuttle, L. Zhu, D.A. Berthold, P. Král, C.M. Rienstra, C.J. Murphy, Control of protein orientation on gold nanoparticles, J. Phys. Chem. C 119 (2015) 21035–21043, https://doi.org/10.1021/ACS.JPCC.5B07701/SUPPL_FILE/JP5B07701_SI_001.PDF.
[3] K. Siriwardana, A. Wang, K. Vangala, N. Fitzkee, D. Zhang, Probing the effects of cysteine residues on protein adsorption onto gold nanoparticles using wild-type and mutated GB3 proteins, Langmuir 29 (2013) 10990–10996, https://doi.org/10.1021/LA402239H/SUPPL_FILE/LA402239H_SI_001.PDF.
[4] Greg Hermanson, Bioconjugate Techniques, second ed., Academic Press, 2008.
[5] A.J. Verkleij, J.L.M. Leunissen, Immuno-gold-labeling in Cell Biology, CRC Press, 1989.
[6] I. Lynch, K.A. Dawson, Protein-nanoparticle interactions, Nano Today 3 (2008) 40–47, https://doi.org/10.1016/S1748-0132(08)70014-8.
[7] S. Khan, A. Gupta, N.C. Verma, C.K. Nandi, Kinetics of protein adsorption on gold nanoparticle with variable protein structure and nanoparticle size, J. Chem. Phys. 143 (2015), https://doi.org/10.1063/1.4934605.
[8] D.V. Sotnikov, A.N. Berlina, V.S. Ivanov, A.V. Zherdev, B.B. Dzantiev, Adsorption of proteins on gold nanoparticles: one or more layers? Colloids Surf. B Biointerfaces 173 (2019) 557–563, https://doi.org/10.1016/J.COLSURFB.2018.10.025.
[9] H. Mateos, G. Palazzo, Colloidal Stability, second ed., Colloid. Found. Nanosci., 2022, pp. 57–83, https://doi.org/10.1016/B978-0-12-822089-4.00001-5.
[10] F. Barbero, L. Russo, M. Vitali, J. Piella, I. Salvo, M.L. Borrajo, M. Busquets-Fité, R. Grandori, N.G. Bastús, E. Casals, V. Puntes, Formation of the protein corona: the interface between nanoparticles and the immune system, Semin. Immunol. 34 (2017) 52–60, https://doi.org/10.1016/J.SMIM.2017.10.001.
[11] P. Altevogt, A. Ben-Ze'ev, N. Gavert, U. Schumacher, H. Schäfer, S. Sebens, Recent insights into the role of L1CAM in cancer initiation and progression, IJC 12 (147) (2020) 3292–3296, https://doi.org/10.1002/ijc.33177.
[12] M. van der Maten, C. Reijnen, J.M.A. Pijnenborg, M.M. Zegers, L1 cell adhesion molecule in cancer, a systematic review on domain-specific functions, Int. J. Mol. Sci. 20 (17) (2019) 1–19, https://doi.org/10.3390/ijms20174180.
[13] D.E. Koppel, Analysis of macromolecular polydispersity in intensity correlation spectroscopy: the method of cumulants, J. Chem. Phys. 57 (2003) 4814, https://doi.org/10.1063/1.1678153.
[14] U. Olsson, P. Schurtenberger, Structure, interactions, and diffusion in a ternary nonionic microemulsion near emulsification failure, Langmuir 9 (1993) 3389–3394, https://doi.org/10.1021/LA00036A011/ASSET/LA00036A011.FP.PNG_V03.
[15] S. Thobhani, S. Attree, R. Boyd, N. Kumarswami, J. Noble, M. Szymanski, R.A. Porter, Bioconjugation and characterisation of gold colloid-labelled proteins, J. Immunol. Methods 356 (2010) 60–69, https://doi.org/10.1016/J.JIM.2010.02.007.
[16] L. Zhang, Y. Mazouzi, M. Salmain, B. Liedberg, S. Boujday, Antibody-gold nanoparticle bioconjugates for biosensors: synthesis, characterization and selected applications, Biosens. Bioelectron. 165 (2020), 112370, https://doi.org/10.1016/J.BIOS.2020.112370.
[17] D.R. Hristov, A.J. Pimentel, G. Ujialele, K. Hamad-Schifferli, The immunoprobe aggregation state is central to dipstick immunoassay performance, ACS Appl. Mater. Interfaces 12 (2020) 34620–34629, https://doi.org/10.1021/acsami.0c08628.
[18] S. Okyem, O. Awotunde, T. Ogunlusi, M.B. Riley, J.D. Driskell, Probing the mechanism of antibody-triggered aggregation of gold nanoparticles, Langmuir 37 (2021) 2993–3000, https://doi.org/10.1021/ACS.LANGMUIR.1C00100/SUPPL_FILE/LA1C00100_SI_001.PDF.
[19] P. Sanpui, A. Paul, A. Chattopadhyay, Theranostic potential of gold nanoparticle-protein agglomerates, Nanoscale 7 (2015) 18411–18423, https://doi.org/10.1039/C5NR05805H.
[20] D. Zhang, O. Neumann, H. Wang, V.M. Yuwono, A. Barhoumi, M. Perham, J.D. Hartgerink, P. Wittung-Stafshede, N.J. Halas, Gold nanoparticles can induce the formation of protein-based aggregates at physiological pH, Nano Lett. 9 (2009) 666–671, https://doi.org/10.1021/NL803054H.
[21] Neupane, Y. Pan, S. Takalkar, K. Bentz, J. Farmakes, Y. Xu, B. Chen, G. Liu, S.Y. Qian, Z. Yang, Probing the aggregation mechanism of gold nanoparticles triggered by a globular protein, J. Phys. Chem. C 121 (2017) 1377–1386, https://doi.org/10.1021/ACS.JPCC.6B11963/SUPPL_FILE/JP6B11963_SI_001.PDF.
[22] R. Zsigmondy, Ueber wässrige Lösungen metallischen Goldes, Justus Liebigs Ann. Chem. 301 (1898) 29–54, https://doi.org/10.1002/JLAC.18983010104.
[23] C. Lange, Die Ausflockung kolloidalen Goldes durch cerebrospinale Flüssigkeit bei luetischen Affektionen des zentralen Nervensystems, Zeitschr. Chemother. 1 (1912) 44, https://doi.org/10.1007/BF01830830/METRICS.
[24] F. Green, The colloidal gold reaction of the cerebrospinal fluid, Can. Med. Assoc. J. 15 (1925) 1139. https://www.ncbi.nlm.nih.gov/pmc/articles/PMC1708525/. (Accessed 20 February 2023).
[25] J. Cruickshank, The value and mechanism of the colloidal gold test, Br. J. Exp. Pathol. 1 (1920) 71. https://www.ncbi.nlm.nih.gov/pmc/articles/PMC2047646/. (Accessed 20 February 2023).
[26] E.A. Kabat, F.M. Hanger, D.H. Moore, H. Landow, The relation of cephalin flocculation and colloidal gold reactions to the serum proteins, J. Clin. Invest. 22 (1943) 563, https://doi.org/10.1172/JCI101427.
[27] J. Bernsohn, E.K. Borman, Proteins in the colloidal gold reaction, J. Clin. Invest. 26 (1947) 1026–1030, https://doi.org/10.1172/JCI101869.
[28] M. Oliveira-Rodríguez, E. Serrano-Pertierra, A. Costa García, S. López Martín, M. Yáñez Mo, E. Cernuda-Morollón, M.C. Blanco-López, Point-of-care detection of extracellular vesicles: sensitivity optimization and multiple-target detection, Biosens. Bioelectron. 87 (2017) 38–45, https://doi.org/10.1016/j.bios.2016.08.001.
[29] S. Saito, J. Hasegawa, N. Kobayashi, T. Tomitsuka, S. Uchiyama, K. Fukui, Effects of ionic strength and sugars on the aggregation propensity of monoclonal antibodies: influence of colloidal and conformational stabilities, Pharm. Res. (N. Y.) 30 (2013) 1263–1280, https://doi.org/10.1007/S11095-012-0965-4.
[30] N. Skar-Gislinge, M. Ronti, T. Garting, C. Rischel, P. Schurtenberger, E. Zaccarelli, A. Stradner, A colloid approach to self-assembling antibodies, Mol. Pharm. 16 (2019) 2394–2404, https://doi.org/10.1021/ACS.MOLPHARMACEUT.9B00019/ASSET/IMAGES/MEDIUM/MP-2019-000193_M028.GIF.
[31] H. Oyama, H. Koga, T. Tadokoro, K. Maenaka, A. Shiota, M. Yokoyama, M. Noda, T. Torisu, S. Uchiyama, Relation of colloidal and conformational stabilities to aggregate formation in a monoclonal antibody, J. Pharmaceut. Sci. 109 (2020) 308–315, https://doi.org/10.1016/j.xphs.2019.10.038.
[32] B. Frka-Petesic, D. Zanchi, N. Martin, S. Carayon, S. Huille, C. Tribet, Aggregation of antibody drug conjugates at room temperature: SAXS and light scattering evidence for colloidal instability of a specific subpopulation, Langmuir 32 (2016) 4848–4861, https://doi.org/10.1021/ACS.LANGMUIR.6B00653/SUPPL_FILE/LA6B00653_SI_001.PDF.
[33] G. Ruiz, N. Ryan, K. Rutschke, O. Awotunde, J.D. Driskell, Antibodies irreversibly adsorb to gold nanoparticles and resist displacement by common blood proteins, Langmuir 35 (2019) 10601–10609, https://doi.org/10.1021/ACS.LANGMUIR.9B01900.
[34] O. Awotunde, S. Okyem, R. Chikoti, J.D. Driskell, Role of free thiol on protein adsorption to gold nanoparticles, Langmuir 36 (2020) 9241–9249, https://doi.org/10.1021/ACS.LANGMUIR.0C01550/SUPPL_FILE/LA0C01550_SI_001.PDF.
[35] W.P. Jencks, Binding energy, specificity, and enzymic catalysis: the circe effect, Adv. Enzymol. Relat. Area Mol. Biol. 43 (1975) 219–410, https://doi.org/10.1002/9780470122884.CH4.
[36] M.Y. Mulla, E. Tuccori, M. Magliulo, G. Lattanzi, G. Palazzo, K. Persaud, L. Torsi, Capacitance-modulated transistor detects odorant binding protein chiral interactions, Nat. Commun. 61 (6) (2015) 1–9, https://doi.org/10.1038/ncomms7010, 2015.
[37] G. Palazzo, H. Mateos, D. Berti, Diffusion, Aggregation and Electrokinetics, Colloid. Found. Nanosci., 2022, pp. 201–225, https://doi.org/10.1016/B978-0-12-822089-4.00006-4.